

Nonlinear magnon transport in bilayer van der Waals antiferromagnetsRohit Mukherjee^{1,*}, Sonu Verma^{2,†} and Arijit Kundu^{1,‡}¹*Department of Physics, Indian Institute of Technology Kanpur, Kanpur 208 016, India*²*Center for Theoretical Physics of Complex Systems, Institute for Basic Science (IBS), Daejeon 34126, Korea*

(Received 4 April 2023; revised 25 May 2023; accepted 30 May 2023; published 27 June 2023)

In this paper, we study the Berry curvature induced linear and nonlinear magnon transport in bilayer van der Waals antiferromagnets, where we deduce forms for the spin and energy currents within the semiclassical Boltzmann formalism under the relaxation time approximation. Even in the absence of the Dzyaloshinskii-Moriya interaction, if we turn on the layer dependent electrostatic doping (ED) potential and anisotropy in the Heisenberg interactions, the linear response remains zero, whereas we obtain a nonzero nonlinear thermal Hall response resulting from higher moments of the Berry curvature. We show that there is a sign reversal of nonlinear thermal Hall conductivity with varying strength of ED potential, which can be potentially useful in spin based technologies. We also comment on the momentum and temperature dependence of the relaxation time, which can influence the transport properties.

DOI: [10.1103/PhysRevB.107.245426](https://doi.org/10.1103/PhysRevB.107.245426)**I. INTRODUCTION**

Anomalous transport signatures as a consequence of the presence of Berry phase of electronic systems have been studied extensively in the past [1–4]. Berry phase driven non-vanishing transport signatures in the linear response regime requires broken time-reversal symmetry (TRS), thus, such anomalous transport has been under intense investigation, especially, in quantum Hall systems [5–10]. It is recently understood that even in time-reversal symmetric systems signatures of Berry curvature and other band geometric quantities can appear beyond the linear response. In particular, in a time-reversal symmetric but inversion broken system, due to the presence of Berry curvature dipole (BCD) in the reciprocal space, there can be nontrivial electrical as well as optical response in the nonlinear regime [11–16]. Numerous studies have been carried out in the recent past of BCD related anomalous transport, which include nonlinear anomalous Hall [17–19], Nernst [20–22], and thermal Hall effects [23].

In similarity to electronic systems, Berry curvature plays an important role in the transport properties of magnetic systems, where the transport is carried by quantized spin wave excitations or the magnons [24,25]. In magnetic systems, the presence of the Dzyaloshinskii-Moriya interactions (DMI) among the spins can generate complex hopping elements in the effective magnon Hamiltonian that makes the magnon bands topological, and hence, one finds the linear response coefficients to be nonzero [26–28]. In the absence of DMI, Berry curvature related transport appear only in the nonlinear response regime, as in the case of electronic systems, where the responses are due to the higher moments of Berry

curvature. There are a few recent studies that address this problem, especially, in spin Seebeck effect [29], spin Nernst effect [30], and optical responses [31,32], but there exists no study of thermal Hall response in the nonlinear regime of van der Waals spin systems, as far our knowledge.

In this paper, we investigate linear as well as nonlinear responses of the magnons in presence a temperature gradient in the semiclassical Boltzmann transport framework, where we find that the nonlinear thermal Hall response can also be attributed to the presence BCD. We apply our calculation in a bilayer van der Waals honeycomb antiferromagnet with anisotropic Heisenberg interactions under the presence of a layer-dependent electrostatic doping potential (ED). Antiferromagnetic honeycomb lattices are excellent platforms for exploring magnon transport properties as these systems support collinear ground states. Previous work on honeycomb lattice antiferromagnet MnPS₃ showed the existence of linear spin Nernst current in the presence of DMI interaction [26,27]. Both for single-layer and bilayer honeycomb lattices, the linear thermal Hall current remains zero due to a global time-reversal symmetry. Recent neutron scattering experiments [33] suggest that MnPS₃ has effectively zero DMI. Thus, one of the possible explanations for the observed magnon Nernst [34] response can be explained by the Berry curvature dipole induced nonlinear currents, which was studied in a recent paper [30], and other possible mechanisms include the magnon-magnon and magnon-phonon coupling [35]. In our study, with finite ED, even in the absence of DMI, we obtain an anisotropy induced nonlinear magnon thermal Hall response, while the total nonlinear magnon spin Nernst current remains zero. Interestingly, we also find a sign reversal of the nonlinear Hall conductivity with increasing strength of ED, which can have potential applications in spintronics.

In addition to the nonlinear response, we also study the linear spin Nernst response in the same system with DMI

*rohitmk@iitk.ac.in

†sonu.vermaiitk@gmail.com

‡kundua@iitk.ac.in

and Heisenberg interactions terms up to the third order (i.e., keeping J_1 , J_2 , as well as J_3 hoppings). We comment on the possible temperature and momentum dependence of the magnon scattering time, leading to finite lifetime of these modes and their effects in the nonlinear transport properties.

Our results show a direct control of the responses of these magnetic systems by means of electrical doping, an emerging area of research with potential for application in quantum devices [36,37]. The recent advance in the field of van der Waals heterostructures has also opened new avenues for such electrical control of magnetism [38]. Application of electrostatic doping (ED) technique has already been used to tune the local moments in atomically thin bilayer systems such as CrBr₃ [39] and CrI₃ [40].

Before we present details of the study, we note that the Boltzmann transport theory is based on semiclassical wavepacket dynamics, where the energy carriers are localized wavepackets that remain in a single energy band and it disregards the impact of multiband coherence effects [41,42]. Taking in account multiband effects, which is beyond the scope of the Boltzmann theory, in addition to the extrinsic nonlinear Hall coefficient, which is proportional to the lifetime of the quasiparticles, one is expected to get another contribution that is intrinsic and independent of any scattering mechanism [43–45].

This paper is organized as follows: In Sec. II, we present the expression for the linear and nonlinear magnon spin Nernst and Hall coefficients by invoking semiclassical Boltzmann transport formalism. Next in Sec. III, we introduce the model spin Hamiltonian, where we study different transport coefficients. In Sec. IV, we provide the details of the numerical simulations and discuss the results. We conclude with further discussions and a summary in Sec. V.

II. FORMALISM

For the dynamics of quantum particles in a lattice, such as electron (or magnon), we need the information of their dispersion as well as the Berry curvature of the Bloch bands [26]. The various transport properties can get considerably modified due to the presence of nontrivial Berry curvature (BC). The general properties of the Berry curvature of the band can be constrained by symmetry consideration. Under the time-reversal operation, the Berry curvature transforms as $\Omega^z(\vec{k}) \rightarrow -\Omega^z(-\vec{k})$; on the other hand under the inversion $\Omega^z(\vec{k}) \rightarrow \Omega^z(-\vec{k})$ [21]. Thus, for a system with both the TRS and inversion symmetry, the Berry curvature vanishes identically over the whole Brillouin zone. The Chern number can be calculated by integrating the Berry curvature over the first Brillouin zone,

$$C_n = \frac{1}{2\pi} \int_{\text{BZ}} d^2k \Omega_n^z(\vec{k}). \quad (1)$$

We consider a magnon wave packet, which is localized around the center, r_c , k_c , in the real and the momentum space, respectively. The dynamics of the wavepacket is described by the semiclassical equations of motion (the suffix c is omitted for brevity), which include an anomalous term due to the

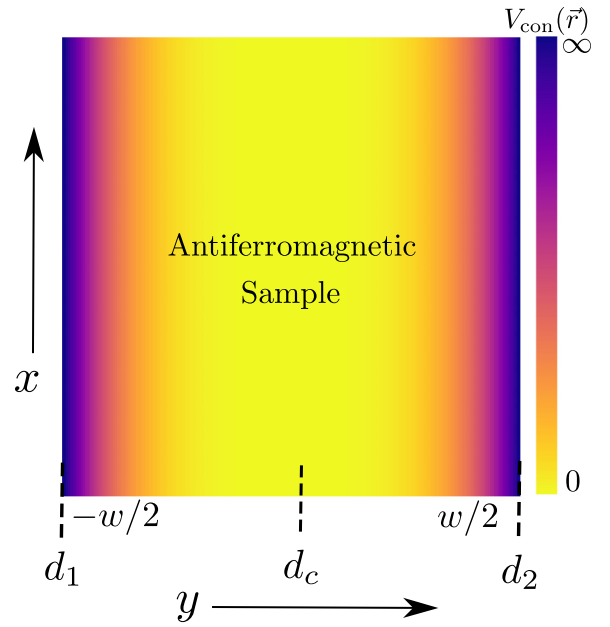


FIG. 1. Setup used for the calculation of edge current in x direction. d_c and d_1, d_2 are chosen well inside and outside the sample, respectively. The confining potential restricts the magnon wavepackets within the sample and its gradient exerts a force on the magnons, which are described by Eq. (3).

Berry curvature [42],

$$\dot{\vec{r}} = \frac{1}{\hbar} \frac{\partial E_n(\vec{k})}{\partial \vec{k}} - \dot{\vec{k}} \times \vec{\Omega}_n(\vec{k}), \quad (2)$$

and

$$\hbar \dot{\vec{k}} = -\vec{\nabla} V_{\text{con}}(\vec{r}), \quad (3)$$

here n is the band index, $E_n(\vec{k})$ and $\vec{\Omega}_n(\vec{k})$ are the energy and the Berry curvature of the n th magnon band in the momentum space, respectively. The geometry we have is shown in Fig. 1, where we would like to find the current in the x direction in response to a small temperature gradient in the y direction. For the calculation of current, we follow the same line of derivation given in Ref. [42]. The first term of the Eq. (2) describes the usual group velocity and the second term is the anomalous velocity arising from the Berry curvature of the magnon bands. In electronic systems, the right-hand side of Eq. (3) is usually the Lorentz force, but as the magnons are neutral quasiparticles, the force term can only be induced by a confining potential $V_{\text{con}}(\vec{r})$, which we consider to be present only near the boundary of the antiferromagnetic sample. The confining potential restricts the magnon wavepacket within the sample and its gradient exerts the confining force. For the validity of Eqs. (2) and (3), the spatial variation of the confining potential $V_{\text{con}}(\vec{r})$ should be much slower compared with the size of the magnon wave packet. If w is the width of the sample, then we have

$$V_{\text{con}}(x, d_c) = 0, \quad V_{\text{con}}(x, d_1) = V_{\text{con}}(x, d_2) = \infty \\ \text{with, } d_1 < -w/2 < d_c < w/2 < d_2, \quad (4)$$

where d_c is the center of the sample.

A. Magnon current

The averaged particle current density along the x direction is given by

$$\begin{aligned} J_x &= \frac{1}{w} \int_{d_1}^{d_2} dy j_x(y) \\ &= \frac{1}{w} \int_{d_c}^{d_2} dy j_x(y) + \frac{1}{w} \int_{d_1}^{d_c} dy j_x(y). \end{aligned} \quad (5)$$

Where $j_x(y)$ is the magnon current density in the the x direction, which is y dependent. The confining potential varies slowly along the y direction and $\frac{\partial V_{\text{con}}}{\partial y} \neq 0$ only near $y = \pm w/2$. Thus,

$$\dot{\vec{r}} = -\frac{dV_{\text{con}}(y)}{dy} \hat{y}. \quad (6)$$

The net velocity is then given by

$$\dot{\vec{r}} = \frac{1}{\hbar} \left(\frac{\partial E_n(\vec{k})}{\partial k_x} \hat{x} + \frac{\partial E_n(\vec{k})}{\partial k_y} \hat{y} \right) + \frac{1}{\hbar} \frac{dV_{\text{con}}(y)}{dy} \Omega_n^z(\vec{k}) (\hat{y} \times \hat{z}). \quad (7)$$

The anomalous part of the velocity (second term) gives rise to magnon edge currents at the boundaries of the sample.

The anomalous magnon current density in the x direction is then given by

$$j_x^A(y) = \frac{1}{V} \sum_{n\vec{k}} \rho_n(\vec{k}, T(y)) \frac{1}{\hbar} \frac{dV_{\text{con}}(y)}{dy} \Omega_n^z(\vec{k}), \quad (8)$$

where $\rho_n(\vec{k}, T(y))$ is the nonequilibrium bosonic distribution function of the n th band, $T(y)$ is the temperature as a function of the y coordinate and V is the area of the sample. Here we should mention that, apart from the velocity along the edge due to BC [second term in Eq. (7)], we have another contribution coming from the group velocity [first term in Eq. (7)] of the Bloch bands, so the magnon wavepackets may not move only along the edges. But, what we have written in Eq. (8) is indeed the total magnon edge current when all the magnons in the thermal equilibrium are added up, i.e., $j_x^A(y) \equiv j_x(y)$ [42].

Following the usual procedure, we write down the nonequilibrium distribution function as a sum of equilibrium distribution ($\rho^{(0)}$) and the first-order corrections due to temperature gradient (details of the calculation are given in Appendix A),

$$\begin{aligned} j_x(y) &= \frac{1}{V} \sum_{n\vec{k}} \rho_n^{(0)}(E_n(\vec{k}) + V_{\text{con}}(\vec{r}); T(y)) \frac{1}{\hbar} \frac{dV_{\text{con}}(y)}{dy} \Omega_n^z(\vec{k}) \\ &+ \frac{1}{V} \sum_{n\vec{k}} \rho_n^{(1)}(\vec{k}; T(y)) \frac{1}{\hbar} \frac{dV_{\text{con}}(y)}{dy} \Omega_n^z(\vec{k}). \end{aligned} \quad (9)$$

For the moment, we shall not discuss the first term of the above equation, which is the linear response of the system, instead, we shall focus on the second term, which is responsible for the nonlinear response,

$$j_x^{\text{nl}}(y) = \sum_{n\vec{k}} \frac{1}{V} \rho_n^{(1)}(\vec{k}; T(y)) \frac{1}{\hbar} \frac{dV_{\text{con}}(y)}{dy} \Omega_n^z(\vec{k}). \quad (10)$$

Now we are in a position to calculate the nonequilibrium bosonic distribution function using the semiclassical Boltzmann transport equation under constant relaxation time (τ) approximation [46], given as

$$\dot{\vec{r}} \frac{\partial \rho}{\partial r} + \dot{\vec{k}} \frac{\partial \rho}{\partial k} = -\frac{(\rho - \rho^{(0)})}{\tau}. \quad (11)$$

Writing $\rho = \rho^{(0)} + \rho^{(1)}$ and after some straightforward algebra (given in Appendix A) we get the following form of the first-order correction,

$$\begin{aligned} \rho_n^{(1)} &= \frac{-\tau}{\hbar} \left(-\frac{E_n(\vec{k}) - \mu}{T} \right) \frac{\partial E_n(\vec{k})}{\partial k_y} \frac{\partial \rho^{(0)}}{\partial E_n(\vec{k})} \frac{dT}{dy} \\ &- \frac{\tau}{\hbar} \frac{\partial E_n(\vec{k})}{\partial k_y} \frac{\partial \rho^{(0)}}{\partial V_{\text{con}}} \frac{dV_{\text{con}}}{dy} + \frac{\tau}{\hbar} \frac{dV_{\text{con}}}{dy} \frac{\partial \rho^{(0)}}{\partial k_y}. \end{aligned} \quad (12)$$

While calculating the current we neglect the contribution arising from the second and the third terms of Eq. (12), as they correspond to higher-order corrections [$\mathcal{O}(\nabla T)^3$ and higher].

Now we plug the expression of Eq. (12) into Eq. (9) to get the final form of the net magnon current density for the n th Bloch band,

$$\begin{aligned} j_{n,x}(y) &= \frac{1}{V} \sum_{\vec{k}} \frac{1}{\hbar} \frac{dV_{\text{con}}(y)}{dy} \Omega_n^z(\vec{k}) \rho_n^{(0)} \\ &+ \frac{1}{V} \sum_{\vec{k}} \frac{1}{\hbar} \frac{dV_{\text{con}}(y)}{dy} \Omega_n^z(\vec{k}) \frac{\tau}{\hbar} \frac{E_n(\vec{k}) - \mu}{T} \frac{\partial \rho_n^{(0)}}{\partial k_y} \nabla T, \end{aligned} \quad (13)$$

with $j_x(y) = \sum_n j_{n,x}(y)$, and $\nabla T \equiv \left(\frac{dT}{dy} \right)$.

Following further calculations (see Appendix A), we arrive at the following expression of the net averaged current density of the n th band:

$$\begin{aligned} J_{n,x} &= \frac{k_B}{V} \sum_{\vec{k}} \frac{1}{\hbar} \Omega_n^z(\vec{k}) c_1(\rho_n^{(0)}) (\nabla T) \\ &+ \frac{1}{V} \sum_{\vec{k}} \frac{1}{\hbar} \Omega_n^z(\vec{k}) \frac{\tau}{\hbar} \frac{(E_n(\vec{k}) - \mu)^2}{T^2} \frac{\partial \rho_n^{(0)}}{\partial k_y} (\nabla T)^2, \end{aligned} \quad (14)$$

with $J_x = \sum_n J_{n,x}$. Here c_v are defined as

$$\begin{aligned} c_v(\rho_n^{(0)}) &= - \int_{E_n(\vec{k})}^{\infty} (\epsilon\beta)^v (\partial \rho_n^{(0)} / \partial \epsilon) d\epsilon \\ &= \int_0^{\rho_n^{(0)}} \log \left[\left(\frac{1+t}{t} \right) \right]^v dt. \end{aligned} \quad (15)$$

The first and second terms in Eq. (14) correspond to the linear and nonlinear contributions of magnon current in the x direction under the influence of a temperature gradient in the y direction, respectively. We should note that the second term in Eq. (14) can be recast into the following form:

$$\frac{1}{V} (\nabla T)^2 \sum_{\vec{k}} \frac{\tau}{\hbar^2 T} c_1(\rho_n^{(0)}) \frac{\partial}{\partial k_y} [E_n(\vec{k}) \Omega_n^z], \quad (16)$$

which also agrees with the result of Ref. [30]. The quantity within the square bracket is termed an extended Berry

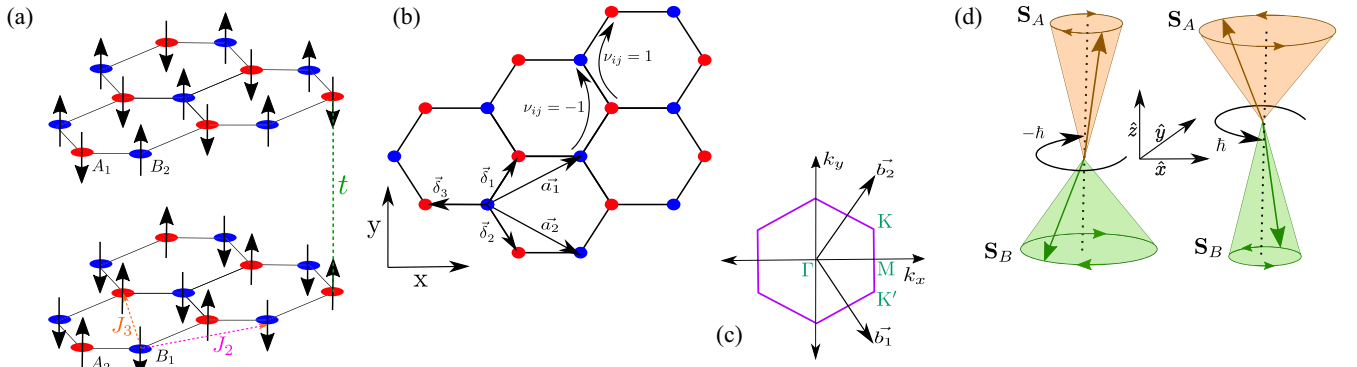


FIG. 2. (a) Schematics of stacked bilayer honeycomb lattice. We are taking antiferromagnetic intra layer Heisenberg interactions up to third order, in plane easy axis anisotropy in both layers, an antiferromagnetic interlayer coupling and oppositely directed ED potentials. Red and blue circles correspond to the A and B sublattices respectively. (b) Schematics of single-layer honeycomb lattice in real space and (c) unit cell in the reciprocal space. The real space and momentum space lattice vectors are also marked. (d) Schematic of the right- and left-handed magnon modes in a single layer. The brown and green arrows represent the precession of spins on A/B sublattices, in each mode the S_z component is different for A and B sublattices during the spin wave precession, as a result, eigenmodes carry opposite spin angular momentum (figure adapted from Ref. [48]).

curvature dipole, which has similar implications to the BCD in electronic systems [20].

B. Nernst, and thermal Hall current

The magnon spin Nernst current is defined as

$$J_x^{\text{Nernst}} = \hbar \sum_n \langle S_n^z \rangle J_{n,x}, \quad (17)$$

where $\langle S_n^z \rangle$ is the expectation value of \hat{S}^z operator in n th magnon band. Energy current for n th band is simply given by (see Appendix A)

$$J_{n,x}^{\text{Energy}} = \frac{k_B^2 T}{\hbar V} \sum_{\vec{k}} \Omega_n^z(\vec{k}) c_2(\rho_n^{(0)}) (\nabla T) + \frac{1}{V} \sum_{\vec{k}} \Omega_n^z(\vec{k}) \frac{\tau}{\hbar^2} \frac{(E_n(\vec{k}) - \mu)^3}{T^2} \frac{\partial \rho_n^{(0)}}{\partial k_y} (\nabla T)^2. \quad (18)$$

The net magnon thermal Hall current is defined as the sum of the contribution arising from each band,

$$J_x^{\text{Hall}} = \sum_n J_{n,x}^{\text{Energy}}. \quad (19)$$

We note that these final expressions have similar forms as in the case of fermionic systems [21]. We would like to stress that the definition of thermal Hall current in Eq. (19) is applicable solely to the linear and nonlinear extrinsic currents.

C. Nonvanishing transport coefficients based on symmetry

Now, having arrived at this result, we present a short discussion on the symmetries of the dispersion and the Berry curvature, and their consequences on various terms in Eqs. (14) and (18). For a time-reversal symmetric system, the Berry curvature is an odd function of \vec{k} and the dispersion is an even function of \vec{k} and hence the first terms of both the Eqs. (14) and (18) are odd functions of \vec{k} , thus total contribution will vanish for each band when we sum over the entire BZ. But the second term (which is the nonlinear contribution) for each of the equations are even functions under the exchange $\vec{k} \rightarrow -\vec{k}$ because of the presence of the term $\frac{\partial}{\partial k_y}$, and, as a consequence, the contribution coming from each band can be nonzero when we sum over the entire BZ. Overall spin Nernst current and Hall currents, which are described by Eqs. (17) and (19), respectively, can be nonvanishing depending on the sign of $\langle S_n^z \rangle$ and the symmetry of Berry curvature. Below we take a generic spin Hamiltonian and analyze the above mentioned magnon transport coefficients.

III. VAN DER WAALS HONEYCOMB ANTIFERROMAGNET

We take a stacked bilayer honeycomb lattice as our model Fig. 2(a) to calculate the magnon transport coefficients. We consider a Hamiltonian of the spins consisting of various kinds of spin spin interactions, which are relevant in van der Waals magnets [26,47]. The Hamiltonian is given by

$$H = \sum_{l=1,2} \left(\sum_{\langle i,j \rangle} J_{1,j} \vec{S}_{i,l} \cdot \vec{S}_{j,l} + \sum_{\langle\langle i,j \rangle\rangle} J_2 \vec{S}_{i,l} \cdot \vec{S}_{j,l} + \sum_{\langle\langle\langle i,j \rangle\rangle\rangle} J_3 \vec{S}_{i,l} \cdot \vec{S}_{j,l} \right) + \sum_{\langle i,j \rangle} t \vec{S}_{i,1} \cdot \vec{S}_{j,2} + \sum_{l=1,2} \left(\sum_i \mathcal{K} (S_{i,l}^z)^2 + \sum_i U_l S_{i,l}^z + D \sum_{\langle\langle i,j \rangle\rangle} v_{ij} [\vec{S}_{i,l} \times \vec{S}_{j,l}]_z \right), \quad (20)$$

where $\vec{S}_{i,l}$ stands for the spin operator at site i in the layer $l = 1/2$. The first three terms within the braces consist of an antiferromagnetic Heisenberg interaction up to third order, the fourth term is an antiferromagnetic interlayer coupling (t) between the nearest-interlayer sublattices, the fifth term is an easy axis anisotropy term in each layer (K), the sixth is the layer-dependent electrostatic doping potential (U_l) [47] interaction, and the last term is the intra layer DMI strength (D) among the second-nearest neighbors (the DMI coupling between the nearest-neighbor spins vanishes as the inversion center of the Honeycomb lattice coincides with the center of the link joining the AB sublattice). Sign structure v_{ij} is depicted in Fig. 2(b). Further, we consider anisotropic nearest-neighbor Heisenberg model where $J_{11} \neq J_{12} \neq J_{13}$, which might be induced by pressure in a realistic system [30], whereas in absence of such anisotropy $J_{11} = J_{12} = J_{13} \equiv J_1$. $\vec{\delta}_j$ ($j = 1, 2, 3$) are the set of three vectors that connects the nearest-neighbor sites. An easy axis anisotropy interaction $\mathcal{K} = KS/(2S - 1)$, stabilizes the Néel ordering in the z direction. $U_l = \pm U$ for layer $l = 1/2$, respectively, which can be controlled by external doping of impurity ions.

We proceed by writing down the Hamiltonian in terms of Holstein-Primakoff bosons defined as

$$\text{Sublattice A: } \begin{cases} \text{layer 1: } \hat{S}_{i,1}^z \approx S - \hat{a}_{i,1}^\dagger \hat{a}_{i,1}, & S_{A1}^+ \approx \sqrt{2S}a_1, & S_{A1}^- \approx \sqrt{2S}a_1^\dagger \\ \text{layer 2: } \hat{S}_{i,2}^z \approx -S + \hat{a}_{i,2}^\dagger \hat{a}_{i,2}, & S_{A2}^+ \approx \sqrt{2S}a_2^\dagger, & S_{A2}^- \approx \sqrt{2S}a_2 \end{cases} \quad (21)$$

$$\text{Sublattice B: } \begin{cases} \text{layer 1: } \hat{S}_{j,1}^z \approx -S + \hat{b}_{j,1}^\dagger \hat{b}_{j,1}, & S_{B1}^+ \approx \sqrt{2S}b_1^\dagger, & S_{B1}^- \approx \sqrt{2S}b_1 \\ \text{layer 2: } \hat{S}_{j,2}^z \approx S - \hat{b}_{j,2}^\dagger \hat{b}_{j,2}, & S_{B2}^+ \approx \sqrt{2S}b_2, & S_{B2}^- \approx \sqrt{2S}b_2^\dagger \end{cases} \quad (22)$$

Fourier transformed operators are defined as

$$\begin{bmatrix} \hat{a}_i \\ \hat{b}_i \end{bmatrix} = \frac{1}{\sqrt{N}} \sum_k e^{i\vec{k}\cdot\vec{r}} \begin{bmatrix} \hat{a}_k \\ \hat{b}_k \end{bmatrix}, \quad (23)$$

where N is the number of unit cells. Now the Hamiltonian can be written in the following form:

$$H = \frac{1}{2} \sum_k \Psi^\dagger(\vec{k}) H(\vec{k}) \Psi(\vec{k}) \quad (24)$$

where the full basis is given by

$$\Psi(\vec{k}) = [a_{1,\vec{k}} \ b_{1,\vec{k}} \ a_{1,-\vec{k}}^\dagger \ b_{1,-\vec{k}}^\dagger \ a_{2,\vec{k}} \ b_{2,\vec{k}} \ a_{2,-\vec{k}}^\dagger \ b_{2,-\vec{k}}^\dagger]^T,$$

where a_l (b_l) indicates the bosonic magnon annihilation operator at sublattice A (B) in layer l (details in Appendix B).

Diagonalization and spectrum

Our Hamiltonian in Eq. (20) preserves the rotational symmetry along the z direction (in the spin space). In this case,

$$H_\uparrow(\vec{k}) = \begin{bmatrix} A + F - U + D & 0 & B - iC & t \\ 0 & A + F + U - D & t & B + iC \\ B + iC & t & A + F + U - D & 0 \\ t & B - iC & 0 & A + F - U + D \end{bmatrix}, \quad (28)$$

where $A = S(J_{11} + J_{12} + J_{13} + 3J_3 + t - K)$, $\gamma_{\vec{k}} = S(J_{11}e^{ik_x/\sqrt{3}} + J_{12}e^{-i/2(k_y+k_x/\sqrt{3})} + J_{13}e^{-i/2(-k_y+k_x/\sqrt{3})})$, $g_{\vec{k}} = J_3S(e^{-2ik_x/\sqrt{3}} + 2e^{-ik_x/\sqrt{3}}\cos(k_y))$, $F = J_2S[2(\cos k_y + \cos[-k_y/2 - (\sqrt{3}/2)k_x] + \cos[-k_y/2 + (\sqrt{3}/2)k_x]) - 6]$, $D = 2D_2S[\sin(k_y) + \sin(1/2(k_y + \sqrt{3}k_x)) + \sin(1/2(k_y - \sqrt{3}k_x))]$, $B = \text{Re}[\gamma_{\vec{k}} + g_{\vec{k}}]$, and $C = \text{Im}[\gamma_{\vec{k}} + g_{\vec{k}}]$. The basis for \uparrow sector is given as

$$\Psi'_\uparrow(\vec{k}) = (a_{\vec{k},1} \ b_{\vec{k},2} \ b_{-\vec{k},1}^\dagger \ a_{-\vec{k},2}^\dagger)^T, \quad (29)$$

$[S_{\text{total}}^z, H] = 0$, where $S_{\text{total}}^z = \sum_{l,i} S_{i,l}^z$ is a good quantum number. We make a unitary transformation (W) of our basis such that the Hamiltonian becomes block diagonal with each block corresponding to a fixed S^z sector. With

$$\Psi'(\vec{k}) = W\Psi(\vec{k}),$$

our transformed Hamiltonian becomes

$$H = \frac{1}{2} \sum_k \Psi'^\dagger(\vec{k})(W^{-1})^\dagger H(\vec{k})W^{-1}\Psi'(\vec{k}) = \begin{bmatrix} H_\uparrow & 0 \\ 0 & H_\downarrow \end{bmatrix}, \quad (25)$$

where

$$H_\uparrow = \frac{1}{2} \sum_k \Psi'^\dagger_\uparrow(\vec{k}) H_\uparrow(\vec{k}) \Psi'_\uparrow(\vec{k}), \quad (26)$$

$$H_\downarrow = \frac{1}{2} \sum_k \Psi'^\dagger_\downarrow(\vec{k}) H_\downarrow(\vec{k}) \Psi'_\downarrow(\vec{k}). \quad (27)$$

Here,

and, in a similar fashion, the basis for the \downarrow sector is given by

$$\Psi'_\downarrow(\vec{k}) = (a_{\vec{k},2} \ b_{\vec{k},1} \ b_{-\vec{k},2}^\dagger \ a_{-\vec{k},1}^\dagger)^T. \quad (30)$$

Now, in order to diagonalize the Hamiltonian in Eq. (28), we employ the standard technique of Bogoliubov transformation for quadratic bosonic Hamiltonian [49,50]. We introduce new creation and annihilation magnon operators (α^\dagger/α , β^\dagger/β), such that

$$\Psi'_\uparrow(\vec{k}) = \mathcal{T}_\uparrow \Gamma'_\uparrow(\vec{k}); \Gamma'_\uparrow(\vec{k}) = (\alpha_{\vec{k},1} \ \beta_{\vec{k},2} \ \beta_{-\vec{k},1}^\dagger \ \alpha_{-\vec{k},2}^\dagger)^T. \quad (31)$$

We choose \mathcal{T}_\uparrow such that the matrix $\mathcal{T}_\uparrow^\dagger H_\uparrow(\vec{k})\mathcal{T}_\uparrow$ becomes diagonal with the condition that $\mathcal{T}_\uparrow^\dagger \Sigma_z \mathcal{T}_\uparrow^\dagger = \Sigma_z$ with $\Sigma_z = \sigma_z \otimes I_2$, where σ_z is the Pauli matrix for the spin space and I_2 is the identity in the layer space. The last condition preserves the bosonic commutation rules in the new basis. The elements of the matrix \mathcal{T}_\uparrow can be found from the eigenspectrum of the matrix $\Sigma_z H_\uparrow(\vec{k})$, which is also known as the dynamic matrix. More details of the procedure can be found in Refs. [50,51]. Similarly, we can diagonalize the Hamiltonian for the \downarrow sector. After the diagonalization, we obtain four magnon bands, and corresponding eigenkets $|\alpha_{\vec{k},1}\rangle, |\alpha_{\vec{k},2}\rangle, |\beta_{\vec{k},1}\rangle, |\beta_{\vec{k},2}\rangle$,

$$\begin{aligned} |\alpha_{\vec{k},1}\rangle &= \alpha_{\vec{k},1}^\dagger |0\rangle, & |\beta_{\vec{k},1}\rangle &= \beta_{\vec{k},1}^\dagger |0\rangle, \\ \alpha_{\vec{k},2} |0\rangle &= 0, & \beta_{\vec{k},2} |0\rangle &= 0. \end{aligned} \quad (32)$$

A schematic diagram of the precession of spins in each layer for each magnon mode is depicted in Fig 2(d). For either $D = 0$ or $U = 0$ the Hamiltonian for $H_\uparrow(\vec{k})$ (up-spin sector) and $H_\downarrow(\vec{k})$ (down-spin sector) are related by

$$H_\uparrow(\vec{k}) = H_\downarrow^*(-\vec{k}).$$

The total spin angular momentum can be written as

$$S_{\text{total}}^z = \sum_{i,l=1,2} S_{i,l,A}^z + S_{i,l,B}^z, \quad (33)$$

which we can write as

$$\begin{aligned} S_{\text{total}}^z &= \sum_i (a_{i,1}^\dagger a_{i,1} - a_{i,2}^\dagger a_{i,2} - b_{i,1}^\dagger b_{i,1} + b_{i,2}^\dagger b_{i,2}) \\ &= \sum_k (a_{\vec{k},1}^\dagger a_{\vec{k},1} - a_{\vec{k},2}^\dagger a_{\vec{k},2} - b_{\vec{k},1}^\dagger b_{\vec{k},1} + b_{\vec{k},2}^\dagger b_{\vec{k},2}). \end{aligned} \quad (34)$$

After the block diagonalization, we can write the spin angular momentum in each sector and find its average for the magnon mode α and β ($\Sigma_z = \sigma_z \otimes I_2$),

$$\begin{aligned} S_\uparrow &= \frac{1}{2} \sum_k \Psi_\uparrow^{\dagger} \Sigma_z \Psi_\uparrow' \\ &= \frac{1}{2} \sum_k (\alpha_{\vec{k},1}^\dagger \alpha_{\vec{k},1} + \beta_{\vec{k},2}^\dagger \beta_{\vec{k},2} - \beta_{-\vec{k},1}^\dagger \beta_{-\vec{k},1} - \alpha_{-\vec{k},2}^\dagger \alpha_{-\vec{k},2}), \end{aligned} \quad (35)$$

and, similarly,

$$\begin{aligned} S_\downarrow &= -\frac{1}{2} \sum_k \Psi_\downarrow^{\dagger} \Sigma_z \Psi_\downarrow' \\ &= -\frac{1}{2} \sum_k (\alpha_{\vec{k},2}^\dagger \alpha_{\vec{k},2} + \beta_{\vec{k},1}^\dagger \beta_{\vec{k},1} - \beta_{-\vec{k},2}^\dagger \beta_{-\vec{k},2} - \alpha_{-\vec{k},1}^\dagger \alpha_{-\vec{k},1}). \end{aligned} \quad (36)$$

In each of these blocks, we calculated the expectation value of the total spin operator, which signifies spin momentum locking of the magnon modes having chirality ± 1 , and also, that these expectations are k independent. Interactions like an in-plane easy axis anisotropy or the Kitaev term destroy this spin rotation symmetry around z axis and invalidate these relations.

TABLE I. Model, Eq. (20), with $D \neq 0$ and $U = 0$. In this case the two bands have Chern numbers $C = \pm 1$.

Band n	Energy	$\langle S_z \rangle$	$\Omega_n^z(\vec{k})$
1	$E_1(\vec{k})$	+1	$+\Omega_1(\vec{k})$
2	$E_2(\vec{k})$	+1	$-\Omega_1(\vec{k})$
3	$E_1(\vec{k})$	-1	$+\Omega_1(\vec{k})$
4	$E_2(\vec{k})$	-1	$-\Omega_1(\vec{k})$

IV. NUMERICAL RESULTS

A. Dispersion and Berry curvature with $D \neq 0$ and $U = 0$

For a single-layer model, with antiferromagnetic Heisenberg interaction in the presence of single ion anisotropy and DMI coupling, the magnon bands are known to be twofold degenerate [$E_1(\vec{k}) = E_2(\vec{k})$, $E_{1,2}(\vec{k}) \neq E_{1,2}(-\vec{k})$] with opposite Berry curvature [$\Omega_1(\vec{k}) = -\Omega_2(\vec{k})$]. As a consequence, the linear spin Nernst current becomes nonzero but the thermal Hall current remains zero [26], which can be readily understood from our equations (17) and (19), respectively. The same model in a bilayer honeycomb lattice with interlayer antiferromagnetic coupling was also briefly discussed in Ref. [27]. We have studied this particular model [Hamiltonian in Eq. (20) with $U = 0$] under the additional presence of second- and third-nearest neighbor Heisenberg coupling, which was not investigated in earlier literature. In Figs. 3(a) and 3(b) we plot the magnon spectrum along the high symmetry points with zero and nonzero value of DMI strength. In both cases, the bands are doubly degenerate with vanishing energy at Γ point. In contrast to the single-layer model, in this case $E_n(\vec{k}) = E_n(-\vec{k})$. In absence of DMI, the magnon bands touch at the K, K' points. In Fig. 3(c) we also show the momentum resolved Berry curvature, which peaks near the M points. It is clear that the Berry curvature for this case is an even function of the momentum that results in nonzero value of the Chern number (which is ± 1). In Table I we have summarized the symmetries of the dispersion and the Berry curvature for this particular model.

B. Linear magnon transport

In this bilayer model, the linear spin Nernst current is enhanced compared to the single layer. Although the bands are topologically nontrivial, the thermal Hall current remains zero due to a global time-reversal symmetry [27]. We neglect the nonlinear part of the Eq. (17) and write down $J_x^{\text{lin, Nernst}} = I_{\text{Nernst}}^{\text{lin}} \nabla T$ [see details in Appendix A, Eq. (A13)]. In Fig. 4 we plot $I_{\text{Nernst}}^{\text{lin}}$ as a function of temperature for different values of DMI strength, as well as, J_2 and J_3 . For the increasing value of D the linear spin Nernst current increases. As a function of temperature, it starts from zero, then increases, and finally saturates. As we increase J_2 the nearest-neighbor spins get frustrated, which helps noncollinear configurations, in contrast, J_3 stabilizes the Néel ordering. This is the reason why for constant D , the linear Nernst coefficient increases with increasing J_2 but decreases with J_3 . From the perspective of magnon dispersion, with increasing J_2 the interband gaps between the magnon bands at M points increase; in contrast,

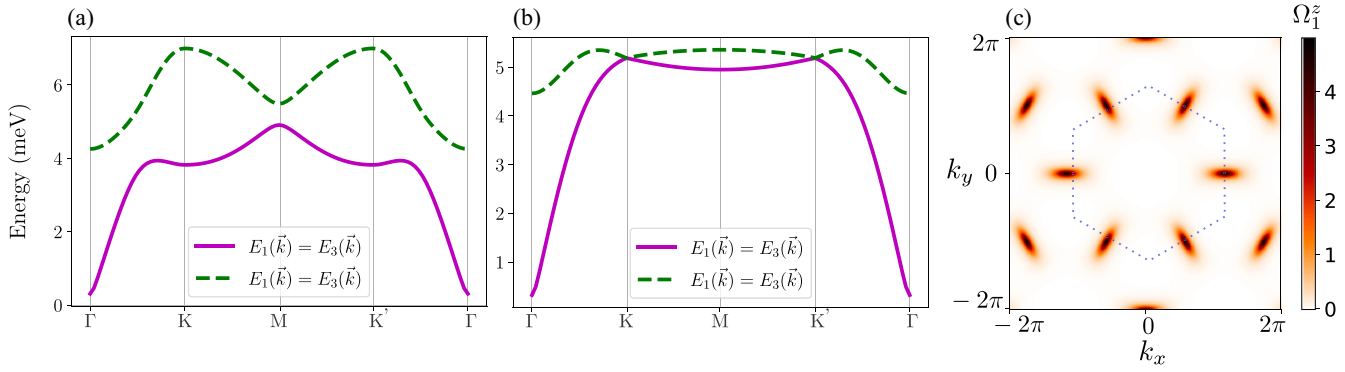


FIG. 3. Model with $U = 0$: The dispersion along the high symmetry points and the Berry curvature (lowest magnon band) for a model with Heisenberg interaction under the presence of the second-nearest neighbor DM and easy axis anisotropy. Parameters for (a) and (c): $S = 1$, $J_1 = 1.5$ meV, $J_2 = 0.05J_1$, $J_3 = 0.1J_1$, $K = -0.0086$ meV, $U = 0$, $t = 1.0$ meV, $D = 0.3$ meV. The values of the parameters are close to the real values in most of the van der Waals magnets [52] from the predictions by *ab initio* calculations. The dispersion is highly anisotropic as a function of k . With $D = 0$ there is a band touching near K , K' points (b). The density plot of the Berry curvature shows that it is highly concentrated near M points and topological charges for each M point is $1/3$. The dotted lines indicate the first Brillouin zone.

when J_3 is increased the gaps decrease, leading to a vanishing measure of the Berry curvature at the M points, and, as a result, the linear Nernst current decreases with increasing J_3 . In this analysis, we have kept the values of J_2 to be small enough so that the system is still in an ordered state and the spin wave theory is a valid approximation [50]. Our analysis reveals that the change in magnitude of the linear spin Nernst coefficient by varying second- and third-nearest neighbor Heisenberg coupling is much larger in comparison to the change due to D . In passing, we comment that the nonzero spin Nernst current observed in the material $MnPS_3$ was originally explained using these models, but recent neutron experiments done on the same material [33] suggests that the observed value of D is too small to explain the magnitude of linear spin Nernst current. Thus, the observed Nernst effect may be related to other possible mechanisms, such as the magnon magnon and magnon phonon interaction [53] and nonlinear effects.

C. Dispersion and Berry curvature with $U \neq 0$ and $D = 0$

In a very recent paper [30], the authors have shown that in a single-layer honeycomb lattice, even without DMI, in

the presence of anisotropic Heisenberg exchange interaction, one can get nonvanishing magnon spin Nernst current. In this case, the dispersion and Berry curvature holds the following identities: $E_1(\vec{k}) = E_2(\vec{k})$, $E_{1,2}(\vec{k}) = E_{1,2}(-\vec{k})$ and $\Omega_1(\vec{k}) = -\Omega_2(\vec{k})$, because of this symmetry, the linear spin Nernst and thermal Hall current remains zero. In the following, we investigate the nonlinear response in a stacked bilayer honeycomb lattice by introducing a layer-dependent electrostatic potential that can be externally controlled by changing the amount of doping [38–40]. The Hamiltonian is given by Eq. (20) with $D = 0$ and in addition, we have a strain induced anisotropic nearest-neighbor coupling, $J_{11} \neq J_{12} \neq J_{13}$.

Now without the application of strain (i.e., when $J_{11} = J_{12} = J_{13}$), near the K, K' points the derivatives of magnon dispersions are vanishingly small, making their product $\Omega_n(\vec{k})\partial E_n(\vec{k})/\partial k_y$ almost zero near each of those points. However, under the application of strain, the maximum value of Berry curvature and the derivative of dispersion shifts in the $k_x - k_y$ plane in a nonequivalent way that makes their product nonzero. This is a necessary condition to get a large nonvanishing nonlinear response in our particular model. Such anisotropic nearest-neighbor coupling can be generated by

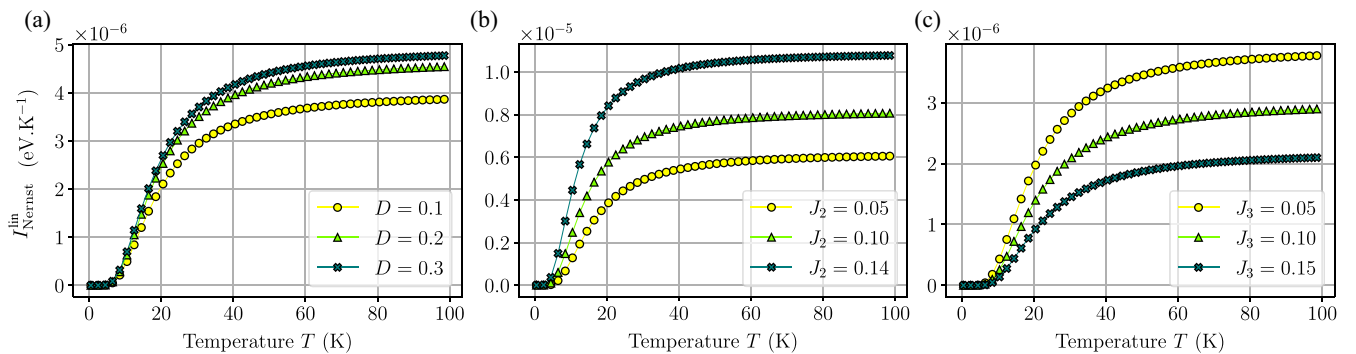


FIG. 4. Linear Nernst current as a function of temperature for different values of D , J_2 , and J_3 . The coefficient of linear Nernst current is defined in Eq. (A13). The Chern number of the bands are $C = \pm 1$, which indicates that the bands are topologically nontrivial. In (a) J_2 and J_3 are kept zero, in (b) and (c) $D=0.3$ meV, for all plots $t = 1.0$, the other parameters are the same as Fig. 3. In a typical experimental setup $\nabla T = 10^{-6}$ K/nm.

TABLE II. Model, Eq. (20), with $U \neq 0$ and $D = 0$.

Band n	Energy	$\langle S_z \rangle$	$\Omega_n^z(\vec{k})$
1	$E_1(\vec{k})$	+1	$+\Omega_1(\vec{k})$
2	$E_2(\vec{k})$	+1	$-\Omega_1(\vec{k})$
3	$E_1(\vec{k})$	-1	$-\Omega_1(\vec{k})$
4	$E_2(\vec{k})$	-1	$+\Omega_1(\vec{k})$

the application of external pressure induced strain [30]. As a passing comment, we want to mention that very high value of ED potential leads to a transition from an antiferromagnetic to a ferromagnetic interlayer coupling even in zero magnetic field [40], so we assume ED potential to be small enough so that the interlayer interaction remains antiferromagnetic in nature. In the Table II we have summarised the symmetries of the dispersion, and Berry curvature for this particular model.

In Fig. 5 we plot the magnon dispersions and the Berry curvature for this model with $J_{11} \neq J_{12} \neq J_{13}$. The spectrum is doubly degenerate where the gaps between the bands at K, K' points are proportional to U . In this model, the maximum contributions to the Berry curvature come from momenta near the K, K' points. The Berry curvature in this case being an odd function of the Bloch momentum, the Chern number of the band is zero.

D. Nonlinear magnon transport

In our case, the inversion symmetry is broken in each layer but it remains intact if we consider both the layers together. From Eq. (17), the total nonlinear magnon spin Nernst current can be written as

$$J_x^{\text{nl, Nernst}} = \frac{\tau(\nabla T)^2}{\hbar V T^2} \sum_{n, \vec{k}} \langle S_n^z \rangle \Omega_n(\vec{k}) g_1(E_n(\vec{k})),$$

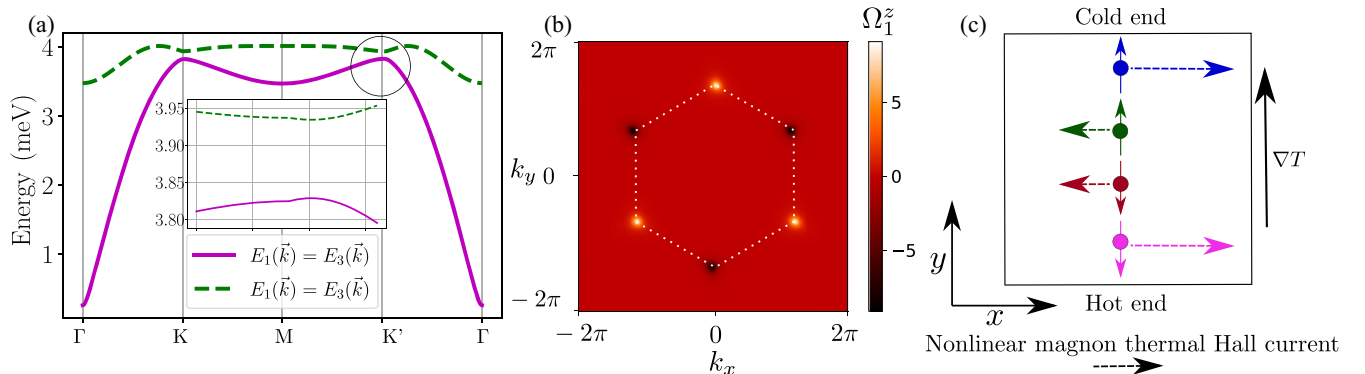


FIG. 5. Model with $D = 0$: [(a),(b)] The band structure along the high symmetry points and the Berry curvature of the lowest magnon band. Parameters of the plots are as follows: $S = 1$, $J_{11} = 1.0$ meV, $J_{12} = 1.05$ meV, and $J_{13} = 0.95$ meV, $K = -0.0086$ meV, $D = 0$, $t = 1$ meV, $U = 0.05$ meV, $J_2 = 0$, $J_3 = 0$. Bands are twofold degenerate and the gap at K, K' points are of the order of twice the ED potential. The Berry curvature for the bands picks up near the K and K' points and is an odd function of momentum, resulting in a zero Chern number. (c) Schematic of nonlinear magnon thermal Hall current. Different colors and the arrows represent different magnon modes and their spin S^z quantum numbers, respectively. The length of the arrows from the center represents the magnitude of the corresponding particle current. We have a pair of modes having the same magnitude of Hall current in the same direction but with opposite S^z , as a result, we have a nonzero nonlinear thermal Hall current with vanishing nonlinear spin Nernst current.

where $g_1(E_n(\vec{k})) = E_n(\vec{k})^2 \partial \rho_n^{(0)} / \partial k_y$ and the Berry curvature $\Omega_n(\vec{k})$ are both odd functions of momentum. As a result, the nonlinear Nernst response for the individual magnon bands will be nonzero but when we sum over the bands they cancel each other out. It means that we have counterpropagating nonlinear spin currents.

Interestingly, the nonlinear thermal Hall response is nonzero in this case. From the Eq. (19), the total nonlinear magnon thermal Hall current can be expressed as

$$J_x^{\text{nl, Energy}} = \frac{\tau(\nabla T)^2}{\hbar^2 V T^2} \sum_{n, \vec{k}} \Omega_n(\vec{k}) g_2(E_n(\vec{k})),$$

here, $\Omega_n(\vec{k})$ and $g_2(E_n(\vec{k})) = E_n(\vec{k})^3 \partial \rho_n^{(0)} / \partial k_y$ are both odd under k . The nonlinear magnon thermal Hall response for each band as well as their sum is nonzero. In Fig. 6(a) we plot the nonlinear magnon thermal Hall current [details in the Appendix A, Eq. (A14)] as a function of temperature for different values of U . The thermal Hall coefficient starts from zero and peaks up at a point where the temperature becomes of the order of the energy gap. From Fig. 6(b), it is also clear that with increasing U there is a sign change in the nonlinear Hall current. With increasing temperature, the curves exhibit a diminishing slope, leading to a rightward shift of the points where they intersect the U axis. As U increases, the valence band's influence on the thermal Hall current undergoes a change in sign, resulting in a complete reversal of the total response. These results predict that the nonlinear thermal Hall current can indeed be tuned by external doping and strain induced anisotropy. These are the main results of our current paper.

In our nonlinear Hall response, most of the contribution comes near the K, K' points, near which the group velocities of magnons are of the order $\frac{1}{\hbar} \frac{\partial E}{\partial k} = 7.5 \times 10^{11}$ nm sec $^{-1}$. Typically, the magnon mean free path for an antiferromagnetic sample at 20 K ranges from 1–100 μm [54], this corresponds to a magnon lifetime (τ) is 10^{-7} – 10^{-9} seconds. The

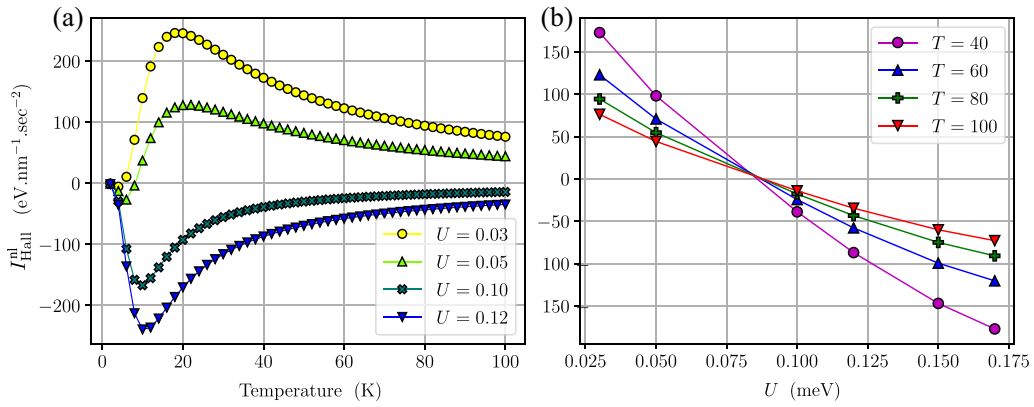


FIG. 6. Nonlinear Hall coefficient defined in Eq. (A14) as a function of temperature and ED potential. We find that, under the presence of strain, there is a sign reversal of the Hall coefficient. For very large anisotropy there is a competition between the Berry curvature density at the Γ , M , and K points. The magnitude of the ED potential should be kept small so that there is no spin flipping transitions. Parameters of the plots are as follows: $S = 1$, $J_{11} = 1.0$ meV, $J_{12} = 1.05$ meV and $J_{13} = 0.95$ meV, $K = -0.0086$ meV, $D = 0$, $t = 1$ meV, $J_2 = 0$, $J_3 = 0$. The relaxation time (τ) of the magnon modes in antiferromagnets are typically of order $10^{-7} - 10^{-9}$ sec.

applied temperature gradient (∇T) for a magnon transport measurement reported by the experiment in Ref. [34] is of the order of 10^{-6} K/nm. The coefficient of nonlinear Hall current we obtain for $U = 0.03$ meV at 20 K is around 250 eV $\text{nm}^{-1} \text{sec}^{-2}$. This is equivalent to a nonlinear thermal Hall current of 250×10^{-7} eV $\text{nm}^{-1} \text{sec}^{-1} \approx 10^{-14}$ W/m, which is in the measurable range. In comparison, the magnitude of the linear magnon thermal Hall conductivity reported in Refs. [53,55] at 20 K is around 10^{-13} W/K. Assuming the same value of the temperature gradient in our case, the value of the linear magnon thermal Hall current is 10^{-10} W/m. We have checked that the order of magnitude estimation is robust against changes of the material parameters.

E. Model with both $U \neq 0$ and $D \neq 0$

We have also analyzed the magnon band structure when both DMI and ED are nonzero (Fig. 7). For this particular case, the twofold degeneracy of the magnon modes is lifted and the dispersion becomes asymmetric about the Γ point (also termed as nonreciprocal magnons) with the formation of Dirac like nodes near the M point. The degree of nonreciprocity of the magnon band structures can be possibly manipulated by changing the direction and magnitude of the external ED potential. As the linear response is already nonzero for this model, we do not show any transport studies of this model

in this paper. The outcome of various magnon transport coefficients for variants of $U + D$ model are summarized in Table III.

F. Momentum and temperature resolved relaxation time

The simplest mechanism through which out of equilibrium magnets can relax is known as Gilbert damping [56–59]. From the Landau-Lifshitz-Gilbert equations, the scattering rate can be written as

$$\Gamma = \frac{\partial \rho}{\partial t} = -\frac{1}{\tau_G} (\rho_{\vec{k}} - \rho_{eq}) = -\frac{2\alpha E(\vec{k})}{\hbar} (\rho_{\vec{k}} - \rho_{eq}), \quad (37)$$

where ρ is the bosonic distribution function, α is the Gilbert damping parameter, and $E(\vec{k})$ is the magnon dispersion. In this mechanism the relaxation time is inversely proportional to the dispersion; as a result, we can expect that at small temperatures, it will modify the magnitude of the different magnon transport coefficients. For example, within the Gilbert relaxation, our nonlinear magnon Hall current will be proportional to $E(\vec{k})^2$ instead of $E(\vec{k})^3$. For higher temperatures, magnon-magnon interactions become important and it can significantly modify the band structures and the wavefunctions. Previous studies [60–62] have confirmed that there is a T^2 dependence on relaxation rates. In our case, this will make the nonlinear Hall current proportional to T^0 in contrast to T^{-2} dependence

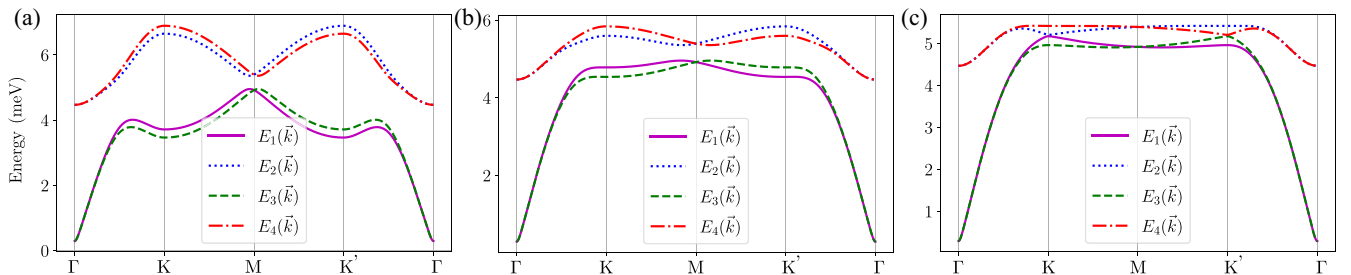


FIG. 7. Evolution of magnon band structures in the $D + U$ model with a varying magnitude of D and U . Parameters are as follows: (a) $U/D = 0.4$, (b) $U/D = 1.2$, (c) $U/D = 6.0$, all the other parameters are same as Fig. 4. It is interesting to note that, in $D + U$ model the valley degeneracy between K, K' points is broken, i.e., the magnon bands have different energies at those two momentum points.

TABLE III. Variants of $D + U$ model and their various transport signatures.

Model	Linear Nernst	Linear Hall	Nonlinear Nernst	Nonlinear Hall
$U \neq 0, D = 0$	✗	✗	✗	✗
$U \neq 0, D = 0 + \text{strain}$	✗	✗	✗	✓
$D \neq 0, U = 0$	✓	✗	✗	✗

under constant relaxation time. This certainly enhances the magnitude of the Hall response at higher temperatures.

V. SUMMARY

In conclusion, we have investigated the linear and nonlinear magnon transport under the presence of various possible spin-spin interactions in a bilayer van der Waals honeycomb magnet within the semiclassical Boltzmann transport theory. We have shown that, even in the absence of Dzyaloshinskii-Moriya interactions (DMI), the presence of anisotropy and electrostatic doping potential (ED) can lead to a nonzero *nonlinear* thermal Hall effect. Interestingly, we have observed a sign reversal of this nonlinear magnon Hall current as a function of the ED potential, which can have the potential for application in spin-based technologies. We have further shown that, in the presence of DMI coupling, the second- and third-nearest Heisenberg interactions play an important role in determining the magnitude of the *linear* magnon spin

Nernst current. We have also commented on the momentum and temperature dependence of the magnon scattering time, which can significantly affect the magnitude of the transport coefficients and their experimental relevance.

ACKNOWLEDGMENTS

R.M. and S.V. thank, for useful communication, Ran Cheng (University of California, Riverside), Vladimir A. Zyuzin (Landau Institute, Moscow), Hiroki Kondo (University of Tokyo), Yutaka Akagi (University of Tokyo). R.M. acknowledges the CSIR (Govt. of India) for financial support. S.V. acknowledge financial support from the Institute for Basic Science in the Republic of Korea through the project IBS R024 D1. We also acknowledge the use of the HPC facility at IIT Kanpur. A.K acknowledges support from the SERB (Govt. of India) via Sanction No. ECR/2018/001443 and CRG/2020/001803, DAE (Govt. of India) via Sanction No. 58/20/15/2019 BRNS, as well as MHRD (Govt. of India) via sanction no. SPARC/2018 2019/P538/SL.

APPENDIX A: SEMICLASSICAL BOLTZMANN TRANSPORT CALCULATION

The semiclassical equations of motion of the magnon Bloch bands are given by

$$\dot{\vec{r}} = \frac{1}{\hbar} \frac{\partial E_n(\vec{k})}{\partial \vec{k}} - \dot{\vec{k}} \times \vec{\Omega}_n(\vec{k}), \quad (\text{A1})$$

$$\hbar \dot{\vec{k}} = -\vec{\nabla} V_{\text{con}}(\vec{r}), \quad (\text{A2})$$

here n is the band index, $E_n(\vec{k})$ is the n th magnon band energy, and $\Omega_n^z(\vec{k})$ is the Berry curvature in momentum space. For the validity of Eqs. (A1) and (A2), the spatial variation of the confining potential $V_{\text{con}}(\vec{r})$ should be much slower compared with the size of the magnon wave packet. Here, we focus on the edge current in the x direction, with a small temperature gradient in the y direction, as an example.

We are specifically interested in the situation when the contribution due to the first term of Eq. (9) (which is linear in ΔT) vanishes due to symmetry considerations. We show below that the second term is proportional to $(\Delta T)^2$, which gives the first-order nonlinear correction,

$$j_{n,x}^{\text{nl}}(y) = \frac{1}{V} \sum_{\vec{k}} \rho_n^{(1)}(\vec{k}; T(y)) \frac{1}{\hbar} \frac{dV_{\text{con}}(y)}{dy} \Omega_n^z(\vec{k}). \quad (\text{A3})$$

Under the relaxation-time approximation, as written in the main text,

$$\dot{\vec{r}} \cdot \frac{\partial \rho}{\partial \vec{r}} + \dot{\vec{k}} \cdot \frac{\partial \rho}{\partial \vec{k}} = -\frac{(\rho - \rho^{(0)})}{\tau},$$

where $\rho^{(0)}$ is the equilibrium distribution function. Let us suppress the suffix n in ρ_n for notational simplicity for the moment. We first calculate the first-order correction, i.e., $\rho^{(1)}$,

$$\dot{\vec{r}} \cdot \frac{\partial \rho^{(0)}}{\partial \vec{r}} + \dot{\vec{k}} \cdot \frac{\partial \rho^{(0)}}{\partial \vec{k}} = -\frac{\rho^{(1)}}{\tau} \quad \left(\frac{\partial \rho^{(0)}}{\partial x} = 0, \quad \frac{\partial \rho^{(0)}}{\partial y} \neq 0 \right),$$

using Eqs. (6) and (7) we can write

$$v_y \frac{\partial \rho^{(0)}}{\partial y} - \frac{1}{\hbar} \frac{dV_{\text{con}}}{dy} \frac{\partial \rho^{(0)}}{\partial k_y} = \frac{-\rho^{(1)}}{\tau} \Rightarrow \frac{1}{\hbar} \frac{\partial E_n(\vec{k})}{\partial k_y} \frac{\partial \rho^{(0)}}{\partial y} - \frac{1}{\hbar} \frac{dV_{\text{con}}}{dy} \frac{\partial \rho^{(0)}}{\partial k_y} = \frac{-\rho^{(1)}}{\tau}. \quad (\text{A4})$$

And we write

$$\frac{\partial \rho^{(0)}}{\partial y} = \frac{\partial \rho^{(0)}}{\partial T} \frac{dT}{dy} + \frac{\partial \rho^{(0)}}{\partial V_{\text{con}}} \frac{dV_{\text{con}}}{dy}. \quad (\text{A5})$$

From Eq. (A4), we can write

$$\frac{\partial E_n(\vec{k})}{\partial k_y} \frac{\partial \rho^{(0)}}{\partial T} \frac{dT}{dy} + \frac{\partial E_n(\vec{k})}{\partial k_y} \frac{\partial \rho^{(0)}}{\partial V_{\text{con}}} \frac{dV_{\text{con}}}{dy} - \frac{dV_{\text{con}}}{dy} \frac{\partial \rho^{(0)}}{\partial k_y} = -\frac{\hbar}{\tau} \rho^{(1)}. \quad (\text{A6})$$

The equilibrium bosonic distribution is given by

$$\rho^{(0)} = \frac{1}{e^{\beta(E_n(\vec{k}) - \mu)} - 1}$$

$$\Rightarrow \frac{\partial \rho^{(0)}}{\partial T} = \frac{-1}{(e^{\beta(E_n(\vec{k}) - \mu)} - 1)^2} \left(-\frac{E_n(\vec{k}) - \mu}{k_B T^2} \right), \quad \frac{\partial \rho^{(0)}}{\partial E_n(\vec{k})} = \frac{-1}{(e^{\beta(E_n(\vec{k}) - \mu)} - 1)^2} \left(\frac{1}{k_B T} \right).$$

So we have

$$\frac{\partial \rho^{(0)}}{\partial T} = \left(-\frac{E_n(\vec{k}) - \mu}{T} \right) \frac{\partial \rho^{(0)}}{\partial E_n(\vec{k})},$$

this expression enables us to write $\rho^{(1)}$ in compact notation,

$$\rho^{(1)} = \frac{-\tau}{\hbar} \left(-\frac{E_n(\vec{k}) - \mu}{T} \right) \frac{\partial E_n(\vec{k})}{\partial k_y} \frac{\partial \rho^{(0)}}{\partial E_n(\vec{k})} \frac{dT}{dy} - \frac{\tau}{\hbar} \frac{\partial E_n(\vec{k})}{\partial k_y} \frac{\partial \rho^{(0)}}{\partial V_{\text{con}}} \frac{dV_{\text{con}}}{dy} + \frac{\tau}{\hbar} \frac{dV_{\text{con}}}{dy} \frac{\partial \rho^{(0)}}{\partial k_y}. \quad (\text{A7})$$

Now, the force acting on the magnon wavepacket can be written in a perturbative series of the confining potential (V_{con}), if we take dV_{con}/dy correction term in the expansion of $\rho^{(1)}$, then it comes with order $(dV_{\text{con}}/dy)^2$ in the expression of the nonlinear current, which can be neglected in comparison to (dV_{con}/dy) order. Thus, we write

$$\rho^{(1)}(\vec{k}, T(y)) \approx \frac{\tau}{\hbar} \frac{E_n(\vec{k}) - \mu}{T} \frac{\partial \rho^{(0)}}{\partial k_y} \left(\frac{dT}{dy} \right). \quad (\text{A8})$$

The expression of nonlinear current density for each band can be written as (putting back the suffix n),

$$J_{n,x}^{\text{nl}}(y) = \frac{1}{V} \sum_{\vec{k}} \frac{1}{\hbar} \frac{dV_{\text{con}}(y)}{dy} \Omega_n^z(\vec{k}) \frac{\tau}{\hbar} \frac{E_n(\vec{k}) - \mu}{T} \frac{\partial \rho_n^{(0)}}{\partial k_y} \left(\frac{dT}{dy} \right).$$

The total averaged nonlinear current in x direction is given by the integral of the current density

$$J_{n,x}^{\text{nl}} = \frac{1}{V} \sum_{\vec{k}} \frac{1}{\hbar} \Omega_n^z(\vec{k}) \frac{\tau}{\hbar} \frac{E_n(\vec{k}) - \mu}{T} \left(\frac{dT}{dy} \right) \int_0^\infty \frac{1}{w} \left(\frac{\partial \rho_n^{(0)}(E_n(\vec{k}) + V_{\text{con}}(r); T(+w/2))}{\partial k_y} - \frac{\partial \rho_n^{(0)}(E_n(\vec{k}) + V_{\text{con}}(r); T(-w/2))}{\partial k_y} \right) dV_{\text{con}}.$$

This is zero if $T(w/2) = T(-w/2)$. Now using Taylor series approximation we can write

$$\rho_n^{(0)}(T(-y)) = \rho_n^{(0)}(T(y)) - 2y \frac{dT}{dy} \frac{\partial \rho_n^{(0)}}{\partial T}.$$

Thus

$$J_{n,x}^{\text{nl}} = \frac{1}{V} \sum_{\vec{k}} \frac{1}{\hbar} \Omega_n^z(\vec{k}) \frac{\tau}{\hbar} \frac{E_n(\vec{k}) - \mu}{T} \left(\frac{dT}{dy} \right)^2 \int_0^\infty \left(\frac{\partial^2 \rho_n^{(0)}(E_n(\vec{k}) + V_{\text{con}}(r))}{\partial k_y \partial T} \right) dV_{\text{con}}.$$

We have

$$\frac{\partial \rho_n^{(0)}}{\partial k_y} = \frac{\partial \rho_n^{(0)}(E_n(\vec{k}) + V_{\text{con}}(r))}{\partial E_n(\vec{k})} \frac{\partial E_n(\vec{k})}{\partial k_y},$$

and

$$\begin{aligned} J_{n,x}^{\text{nl}} &= \frac{1}{V} \sum_{\vec{k}} \frac{1}{\hbar} \Omega_n^z(\vec{k}) \frac{\tau}{\hbar} \frac{E_n(\vec{k}) - \mu}{T} (\nabla T)^2 \frac{\partial}{\partial T} \int_0^\infty \left(\frac{\partial \rho_n^{(0)}(E_n(\vec{k}) + V_{\text{con}}(r))}{\partial k_y} \right) dV_{\text{con}} \\ &= \frac{\tau (\nabla T)^2}{\hbar T} \sum_{\vec{k}} \frac{1}{V} \frac{1}{\hbar} \Omega_n^z(\vec{k}) \frac{(E_n(\vec{k}) - \mu)^2}{T} \frac{1}{k_B T} \rho^{(0)}(E_n(\vec{k})) (1 + \rho^{(0)}(E_n(\vec{k}))) \frac{\partial E_n(\vec{k})}{\partial k_y}. \end{aligned} \quad (\text{A9})$$

Total nonlinear spin Nernst current is given by

$$J_x^{\text{nl,Nernst}} = \hbar \sum_n \langle S_n^z \rangle J_{n,x}^{\text{nl}}. \quad (\text{A10})$$

The total averaged magnon current for each band including both linear [26,42] and nonlinear contribution is given by

$$J_{n,x} = \frac{k_B}{V} \sum_{\vec{k}} \frac{1}{\hbar} \Omega_n^z(\vec{k}) c_1(\rho_n^{(0)}) (\nabla T) + \frac{1}{V} \sum_{\vec{k}} \frac{1}{\hbar} \Omega_n^z(\vec{k}) \frac{\tau}{\hbar} \frac{(E_n(\vec{k}) - \mu)^2}{T^2} \frac{\partial \rho_n^{(0)}}{\partial k_y} (\nabla T)^2, \quad (\text{A11})$$

the first term is the linear contribution,

$$J_{n,x}^{\text{lin}} = \frac{k_B}{V} \sum_{\vec{k}} \frac{1}{\hbar} \Omega_n^z(\vec{k}) c_1(\rho_n^{(0)}) (\nabla T). \quad (\text{A12})$$

The linear spin Nernst current is given by

$$J_x^{\text{lin,Nernst}} = \hbar \sum_n \langle S_n^z \rangle J_{n,x}^{\text{lin}} = I_{\text{Nernst}}^{\text{lin}} \nabla T, \quad (\text{A13})$$

nonlinear energy current is simply given by

$$J_{n,x}^{\text{nl,Energy}} = \frac{1}{V} \sum_{\vec{k}} \Omega_n^z(\vec{k}) \frac{\tau}{\hbar^2} \frac{(E_n(\vec{k}) - \mu)^3}{k_B T^3} \rho^{(0)}(E_n(\vec{k})) [1 + \rho^{(0)}(E_n(\vec{k}))] \frac{\partial E_n(\vec{k})}{\partial k_y} (\nabla T)^2,$$

the total nonlinear Hall current is given by

$$J_x^{\text{nl,Energy}} = \sum_n J_{n,x}^{\text{nl,Energy}} = \tau \times I_{\text{Hall}}^{\text{nl}}. \quad (\text{A14})$$

APPENDIX B: FURTHER DETAILS OF MODEL

In this Appendix, we provide the details of different kinds of spin-spin interaction under the linear spin wave approximation. We calculate the Heisenberg coupling up to the third order, Dzyaloshinskii-Moriya (DM) coupling in second order (first-order term is zero in honeycomb lattice from symmetry consideration), and in-plane easy axis anisotropy term. We write the terms in a symmetrized fashion.

Real-space lattice unit vectors of the honeycomb lattice are given by (see Fig. 2)

$$\vec{a}_1 = \frac{a}{2}(3, \sqrt{3}), \quad \vec{a}_2 = \frac{a}{2}(3, -\sqrt{3}). \quad (\text{B1})$$

In the following, we set the nearest-neighbor spacing $a = 1/\sqrt{3}$. The re scaled nearest-neighbor lattice vectors are then

$$\vec{\delta}_1 = \frac{1}{2} \left(\frac{1}{\sqrt{3}}, 1 \right), \quad \vec{\delta}_2 = \frac{1}{2} \left(\frac{1}{\sqrt{3}}, -1 \right), \quad \vec{\delta}_3 = \frac{1}{\sqrt{3}} (-1, 0). \quad (\text{B2})$$

The nearest-neighbor terms ($H_H^{(1)}$) without any anisotropy ($J_{11} = J_{12} = J_{13}$) is written in the momentum space as

$$H_H^{(1)} = \frac{J_1 S}{2} \sum_{\vec{k}, \vec{\delta}_i, i=1,2,3} (e^{-i\vec{k} \cdot \vec{\delta}_i} a_{\vec{k}}^\dagger b_{-\vec{k}} + e^{i\vec{k} \cdot \vec{\delta}_i} a_{-\vec{k}}^\dagger b_{\vec{k}} + \text{H. c.}) + \frac{J_1 S}{2} z_1 \sum_k (a_{\vec{k}}^\dagger a_{\vec{k}} + a_{-\vec{k}}^\dagger a_{-\vec{k}} + b_{\vec{k}}^\dagger b_{\vec{k}} + b_{-\vec{k}}^\dagger b_{-\vec{k}}), \quad (\text{B3})$$

where $\vec{\delta}_i$ with $i = 1, 2, 3$ are the three nearest-neighbor lattice vectors connecting A and B sublattices, and the coordination number, $z_1 = 3$ for honeycomb lattice. In the case of anisotropic interaction $J_1 z_1$ is replaced by respective coupling strength. Next-nearest-neighbor Heisenberg interaction ($H_H^{(2)}$) is given by

$$H_H^{(2)} = \frac{J_2 S}{2} \sum_{\vec{k}, \vec{\eta}_i, i=1,2,3} (e^{-i\vec{k} \cdot \vec{\eta}_i} a_{\vec{k}}^\dagger a_{\vec{k}} + e^{i\vec{k} \cdot \vec{\eta}_i} a_{-\vec{k}}^\dagger a_{-\vec{k}} + e^{-i\vec{k} \cdot \vec{\eta}_i} b_{\vec{k}}^\dagger b_{\vec{k}} + e^{i\vec{k} \cdot \vec{\eta}_i} b_{-\vec{k}}^\dagger b_{-\vec{k}} + \text{h.c.}) - J_2 S z_2 \sum_k (a_{\vec{k}}^\dagger a_{\vec{k}} + a_{-\vec{k}}^\dagger a_{-\vec{k}} + b_{\vec{k}}^\dagger b_{\vec{k}} + b_{-\vec{k}}^\dagger b_{-\vec{k}}), \quad (\text{B4})$$

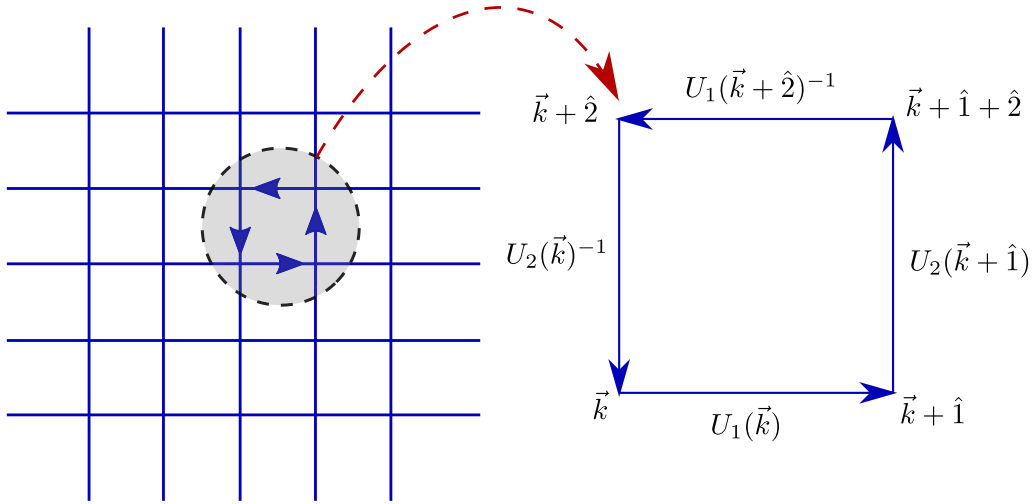


FIG. 8. Schematic picture of the lattice Wilson loop on a discretized square lattice. The U(1) link variables and the path travelled along the closed loop is also shown; for our case the Brillouin zone is a parallelogram.

where $\vec{\eta}_i$ with $i = 1, 2, 3$ are the three next-nearest-neighbor lattice vectors connecting the AA and BB sublattices, $z_2 = 6$ for honeycomb lattice. Third nearest-neighbor Heisenberg interaction ($H_H^{(3)}$) is given by

$$H_H^{(3)} = \frac{J_3 S}{2} \sum_{\vec{k}, \vec{\zeta}_i, i=1,2,3} (e^{-i\vec{k} \cdot \vec{\zeta}_i} a_{\vec{k}}^\dagger b_{-\vec{k}} + e^{i\vec{k} \cdot \vec{\zeta}_i} a_{-\vec{k}} b_{\vec{k}} + h.c.) + \frac{J_3 S}{2} z_3 \sum_k (a_k^\dagger a_{-k} + a_{-k}^\dagger a_k + b_k^\dagger b_{-k} + b_{-k}^\dagger b_k), \quad (\text{B5})$$

where $\vec{\zeta}_i$ with $i = 1, 2, 3$ are the three third-nearest-neighbor lattice vectors connecting AB sublattices, $z_3 = 3$ for honeycomb lattice. The easy axis anisotropy term, which stabilized the ordering along the c axis is given by (H_E),

$$H_E = \sum_i \mathcal{K}(S_i^z)^2 = \frac{KS}{2S-1} \sum_k (a_k^\dagger a_{-k} + a_{-k}^\dagger a_k + b_k^\dagger b_{-k} + b_{-k}^\dagger b_k) \quad (\text{B6})$$

and the DMI coupling term (H_{DM}) between next-nearest-neighbor is given by

$$H_{\text{DM}} = \sum_{i,j} v_{ij} D \hat{z} \cdot (\vec{S}_i \times \vec{S}_j) = \frac{S}{2} \sum_k (\Delta_k a_k^\dagger a_{-k} - \Delta_{-k} a_{-k}^\dagger a_k + \Delta_k b_k^\dagger b_{-k} - \Delta_{-k} b_{-k}^\dagger b_k), \quad (\text{B7})$$

with

$$\Delta_k = 2D[-\sin(\vec{k} \cdot \vec{a}_1) + \sin(\vec{k} \cdot \vec{a}_2) + \sin(\vec{k} \cdot (\vec{a}_1 - \vec{a}_2))].$$

The lattice vectors and the sign conventions in the DM coupling term are given in Fig. 2(b).

APPENDIX C: BERRY CURVATURE FOR THE BOSONIC BOGOLIUBOV DE GENNES (BDG) HAMILTONIAN

In this section, for the sake of completeness we present the computation of the Berry curvature for the bosonic BdG Hamiltonian. We will closely follow the line of derivation given in Ref. [50]. Let us consider the Hamiltonian for the up-spin sector $H_\uparrow(\vec{k})$, which is written in the basis $\Psi_\uparrow^\dagger(\vec{k}) = (a_{\vec{k},1}^\dagger \ b_{\vec{k},2}^\dagger \ b_{-\vec{k},1}^\dagger \ a_{-\vec{k},2}^\dagger)^T$. To satisfy the bosonic commutation relations, the generalized eigenvalue equation for the Hamiltonian $H_\uparrow(\vec{k})$ is written as

$$H_\uparrow(\vec{k})|n(\vec{k})\rangle = E(\vec{k})\Sigma_z|n(\vec{k})\rangle, \quad (\text{C1})$$

where $|n(\vec{k})\rangle$ being a normalized wave function of the n th Bloch band.

The Berry connection $A_\mu(\vec{k})$ ($\mu = 1, 2$) and the corresponding field strength $F_{12}(\vec{k})$, for the n th band, are given by [50,63]

$$A_\mu^n(\vec{k}) = \langle n(\vec{k}) | \partial_\mu \Sigma_z | n(\vec{k}) \rangle, \quad (\text{C2})$$

$$F_{12}^n(\vec{k}) = \partial_1 A_2^n(\vec{k}) - \partial_2 A_1^n(\vec{k}), \quad (\text{C3})$$

This way of computing the Berry curvature leads to numerical errors because of the presence of the derivative in the Brillouin zone (see Fig. 8). Instead, we define an inner product in U(1) link variable of the Bloch band as [63]

$$U_{\hat{\mu}}^n(\vec{k}) \equiv \langle n(\vec{k}) | \Sigma_z | n(\vec{k} + \hat{\mu}) \rangle / N_{\hat{\mu}}^n(\vec{k}) \quad (\text{C4})$$

where

$$N_{\hat{\mu}}^n(\vec{k}) \equiv |\langle n(\vec{k}) | \Sigma_z | n(\vec{k} + \hat{\mu}) \rangle|. \quad (\text{C5})$$

$\hat{\mu} = \hat{1}, \hat{2}$ are the discretized vectors in the direction of the reciprocal lattice vectors. $E(\vec{k})$ has eigenvalues of the form

$$(\epsilon_{\vec{k},\alpha_1}, \epsilon_{\vec{k},\alpha_2}, -\epsilon_{\vec{k},\alpha_1}, -\epsilon_{\vec{k},\alpha_2}). \quad (\text{C6})$$

For particle/hole bands the eigenvector $|n(\vec{k})\rangle$ is normalized as follows:

$$\langle n^{\text{particle}}(\vec{k}) | \Sigma_z | n^{\text{particle}}(\vec{k}) \rangle = 1, \quad (\text{C7})$$

$$\langle n^{\text{hole}}(\vec{k}) | \Sigma_z | n^{\text{hole}}(\vec{k}) \rangle = -1. \quad (\text{C8})$$

The link variables are well defined as long as $N_{\hat{n}}^n(\vec{k}) \neq 0$, which can always be assumed to be the case [64]. The field strength is then numerically approximated as

$$F_{12}^n(\vec{k}) \delta k_1 \delta k_2 \approx \log_e U_1^n(\vec{k}) U_2^n(\vec{k} + \hat{1}) U_1^n(\vec{k} + \hat{2})^{-1} U_2^n(\vec{k})^{-1}, \quad (\text{C9})$$

with

$$-\pi < \frac{1}{i} F_{12}^n(\vec{k}) \delta k_1 \delta k_2 \leq \pi. \quad (\text{C10})$$

Field strength is defined within the principle branch of the logarithm specified in Eq. (C9). This definition of the field strength is gauge invariant. The Berry curvature is written in terms of the field strength as

$$\Omega^n(\vec{k}) = -i F_{12}(\vec{k}). \quad (\text{C11})$$

The Chern number on the lattice corresponding to the n th Bloch band is defined as follows:

$$C_n \equiv \frac{1}{2\pi i} \sum_{\vec{k} \in \text{BZ}} F_{12}(\vec{k}) \delta k_1 \delta k_2. \quad (\text{C12})$$

In similar way we compute the Berry curvature of the Bloch bands corresponding to the $H_{\downarrow}(\vec{k})$ Hamiltonian.

-
- [1] D. Xiao, M.-C. Chang, and Q. Niu, Berry phase effects on electronic properties, *Rev. Mod. Phys.* **82**, 1959 (2010).
- [2] D. Xiao, J. Shi, and Q. Niu, Berry Phase Correction to Electron Density of States in Solids, *Phys. Rev. Lett.* **95**, 137204 (2005).
- [3] D. Xiao, Y. Yao, Z. Fang, and Q. Niu, Berry-Phase Effect in Anomalous Thermoelectric Transport, *Phys. Rev. Lett.* **97**, 026603 (2006).
- [4] W.-L. Lee, S. Watauchi, V. L. Miller, R. J. Cava, and N. P. Ong, Anomalous Hall Heat Current and Nernst Effect in the $\text{CuCr}_2\text{Se}_{4-x}\text{Br}_x$ Ferromagnet, *Phys. Rev. Lett.* **93**, 226601 (2004).
- [5] K. v. Klitzing, G. Dorda, and M. Pepper, New Method for High-Accuracy Determination of the Fine-Structure Constant Based on Quantized Hall Resistance, *Phys. Rev. Lett.* **45**, 494 (1980).
- [6] D. J. Thouless, M. Kohmoto, M. P. Nightingale, and M. den Nijs, Quantized Hall Conductance in a Two-Dimensional Periodic Potential, *Phys. Rev. Lett.* **49**, 405 (1982).
- [7] S. Murakami, N. Nagaosa, and S.-C. Zhang, Dissipationless quantum spin current at room temperature, *Science* **301**, 1348 (2003).
- [8] J. Sinova, S. O. Valenzuela, J. Wunderlich, C. H. Back, and T. Jungwirth, Spin Hall effects, *Rev. Mod. Phys.* **87**, 1213 (2015).
- [9] C. L. Kane and E. J. Mele, Quantum Spin Hall Effect in Graphene, *Phys. Rev. Lett.* **95**, 226801 (2005).
- [10] C. L. Kane and E. J. Mele, Z_2 Topological Order and the Quantum Spin Hall Effect, *Phys. Rev. Lett.* **95**, 146802 (2005).
- [11] I. Sodemann and L. Fu, Quantum Nonlinear Hall Effect Induced by Berry Curvature Dipole in Time-Reversal Invariant Materials, *Phys. Rev. Lett.* **115**, 216806 (2015).
- [12] J. I. Facio, D. Efremov, K. Koepf, J.-S. You, I. Sodemann, and J. van den Brink, Strongly Enhanced Berry Dipole at Topological Phase Transitions in BiTeI , *Phys. Rev. Lett.* **121**, 246403 (2018).
- [13] H. Rostami and M. Polini, Nonlinear anomalous photocurrents in Weyl semimetals, *Phys. Rev. B* **97**, 195151 (2018).
- [14] J.-S. You, S. Fang, S.-Y. Xu, E. Kaxiras, and T. Low, Berry curvature dipole current in the transition metal dichalcogenides family, *Phys. Rev. B* **98**, 121109(R) (2018).
- [15] Y. Zhang, Y. Sun, and B. Yan, Berry curvature dipole in Weyl semimetal materials: An *ab initio* study, *Phys. Rev. B* **97**, 041101(R) (2018).
- [16] O. Matsyshyn and I. Sodemann, Nonlinear Hall Acceleration and the Quantum Rectification Sum Rule, *Phys. Rev. Lett.* **123**, 246602 (2019).
- [17] Z. Z. Du, C. M. Wang, H.-Z. Lu, and X. C. Xie, Band Signatures for Strong Nonlinear Hall Effect in Bilayer WTe_2 , *Phys. Rev. Lett.* **121**, 266601 (2018).
- [18] L.-k. Shi and J. C. W. Song, Symmetry, spin-texture, and tunable quantum geometry in a WTe_2 monolayer, *Phys. Rev. B* **99**, 035403 (2019).
- [19] S. Nandy and I. Sodemann, Symmetry and quantum kinetics of the nonlinear Hall effect, *Phys. Rev. B* **100**, 195117 (2019).
- [20] X.-Q. Yu, Z.-G. Zhu, J.-S. You, T. Low, and G. Su, Topological nonlinear anomalous Nernst effect in strained transition metal dichalcogenides, *Phys. Rev. B* **99**, 201410(R) (2019).
- [21] C. Zeng, S. Nandy, A. Taraphder, and S. Tewari, Nonlinear Nernst effect in bilayer WTe_2 , *Phys. Rev. B* **100**, 245102 (2019).
- [22] P. Kapri, B. Dey, and T. K. Ghosh, Magnus spin Hall and spin Nernst effects in gapped two-dimensional Rashba systems, *Phys. Rev. B* **106**, 035420 (2022).
- [23] C. Zeng, S. Nandy, and S. Tewari, Fundamental relations for anomalous thermoelectric transport coefficients in the nonlinear regime, *Phys. Rev. Res.* **2**, 032066(R) (2020).
- [24] H. Zhang and R. Cheng, A perspective on magnon spin Nernst effect in antiferromagnets, *Appl. Phys. Lett.* **120**, 090502 (2022).
- [25] J. Han, R. Cheng, L. Liu, H. Ohno, and S. Fukami, Coherent antiferromagnetic spintronics, *Nat. Mater.* **22**, 684 (2023).
- [26] R. Cheng, S. Okamoto, and D. Xiao, Spin Nernst Effect of Magnons in Collinear Antiferromagnets, *Phys. Rev. Lett.* **117**, 217202 (2016).
- [27] V. A. Zyuzin and A. A. Kovalev, Magnon Spin Nernst Effect in Antiferromagnets, *Phys. Rev. Lett.* **117**, 217203 (2016).
- [28] Y.-H. Li and R. Cheng, Moiré magnons in twisted bilayer magnets with collinear order, *Phys. Rev. B* **102**, 094404 (2020).

- [29] R. Takashima, Y. Shiomi, and Y. Motome, Nonreciprocal spin Seebeck effect in antiferromagnets, *Phys. Rev. B* **98**, 020401(R) (2018).
- [30] H. Kondo and Y. Akagi, Nonlinear magnon spin Nernst effect in antiferromagnets and strain-tunable pure spin current, *Phys. Rev. Res.* **4**, 013186 (2022).
- [31] I. Proskurin, A. S. Ovchinnikov, J.-I. Kishine, and R. L. Stamps, Excitation of magnon spin photocurrents in antiferromagnetic insulators, *Phys. Rev. B* **98**, 134422 (2018).
- [32] H. Ishizuka and M. Sato, Theory for shift current of bosons: Photogalvanic spin current in ferrimagnetic and antiferromagnetic insulators, *Phys. Rev. B* **100**, 224411 (2019).
- [33] A. R. Wildes, S. Okamoto, and D. Xiao, Search for non-reciprocal magnons in MnPS₃, *Phys. Rev. B* **103**, 024424 (2021).
- [34] Y. Shiomi, R. Takashima, and E. Saitoh, Experimental evidence consistent with a magnon Nernst effect in the antiferromagnetic insulator MnPS₃, *Phys. Rev. B* **96**, 134425 (2017).
- [35] L. Mangeolle, L. Balents, and L. Savary, Phonon Thermal Hall Conductivity from Scattering with Collective Fluctuations, *Phys. Rev. X* **12**, 041031 (2022).
- [36] F. Matsukura, Y. Tokura, and H. Ohno, Control of magnetism by electric fields, *Nat. Nanotechnol.* **10**, 209 (2015).
- [37] Y.-Y. Sun, L.-Q. Zhu, Z. Li, W. Ju, S.-J. Gong, J.-Q. Wang, and J.-H. Chu, Electric manipulation of magnetism in bilayer van der Waals magnets, *J. Phys.: Condens. Matter* **31**, 205501 (2019).
- [38] X. He, Y. Wang, N. Wu, A. N. Caruso, E. Vescovo, K. D. Belashchenko, P. A. Dowben, and C. Binck, Robust isothermal electric control of exchange bias at room temperature, *Nat. Mater.* **9**, 579 (2010).
- [39] C. H. Ahn, A. Bhattacharya, M. Di Ventura, J. N. Eckstein, C. D. Frisbie, M. E. Gershenson, A. M. Goldman, I. H. Inoue, J. Mannhart, A. J. Millis, A. F. Morpurgo, D. Natelson, and J.-M. Triscone, Electrostatic modification of novel materials, *Rev. Mod. Phys.* **78**, 1185 (2006).
- [40] S. Jiang, L. Li, Z. Wang, K. F. Mak, and J. Shan, Controlling magnetism in 2D CrI₃ by electrostatic doping, *Nat. Nanotechnol.* **13**, 549 (2018).
- [41] R. Matsumoto and S. Murakami, Theoretical Prediction of a Rotating Magnon Wave Packet in Ferromagnets, *Phys. Rev. Lett.* **106**, 197202 (2011).
- [42] R. Matsumoto and S. Murakami, Rotational motion of magnons and the thermal Hall effect, *Phys. Rev. B* **84**, 184406 (2011).
- [43] Y. Gao, S. A. Yang, and Q. Niu, Field Induced Positional Shift of Bloch Electrons and Its Dynamical Implications, *Phys. Rev. Lett.* **112**, 166601 (2014).
- [44] A. Sekine and N. Nagaosa, Quantum kinetic theory of thermoelectric and thermal transport in a magnetic field, *Phys. Rev. B* **101**, 155204 (2020).
- [45] T. Stedman and L. M. Woods, Transport theory within a generalized Boltzmann equation for multiband wave packets, *Phys. Rev. Res.* **2**, 033086 (2020).
- [46] G. D. Mahan, *Many-particle physics* (Springer Science & Business Media, New York, 2013).
- [47] D. Ghader, Insights on magnon topology and valley-polarization in 2D bilayer quantum magnets, *New J. Phys.* **23**, 053022 (2021).
- [48] M. W. Daniels, R. Cheng, W. Yu, J. Xiao, and D. Xiao, Nonabelian magnonics in antiferromagnets, *Phys. Rev. B* **98**, 134450 (2018).
- [49] M.-w. Xiao, Theory of transformation for the diagonalization of quadratic Hamiltonians, [arXiv:0908.0787](https://arxiv.org/abs/0908.0787).
- [50] R. Mukherjee, R. Kundu, A. Singh, and A. Kundu, Schwinger-boson mean-field study of the spin-1/2 $J_1 - J_2 - J_\chi$ model in the honeycomb lattice: Thermal Hall signature, *Phys. Rev. B* **107**, 155122 (2023).
- [51] R. Samajdar, S. Chatterjee, S. Sachdev, and M. S. Scheurer, Thermal Hall effect in square-lattice spin liquids: A Schwinger boson mean-field study, *Phys. Rev. B* **99**, 165126 (2019).
- [52] R. Hidalgo-Sacoto, R. I. Gonzalez, E. E. Vogel, S. Allende, J. D. Mella, C. Cardenas, R. E. Troncoso, and F. Munoz, Magnon valley Hall effect in CrI₃-based van der Waals heterostructures, *Phys. Rev. B* **101**, 205425 (2020).
- [53] X. Zhang, Y. Zhang, S. Okamoto, and D. Xiao, Thermal Hall Effect Induced by Magnon-Phonon Interactions, *Phys. Rev. Lett.* **123**, 167202 (2019).
- [54] S. R. Boona and J. P. Heremans, Magnon thermal mean free path in yttrium iron garnet, *Phys. Rev. B* **90**, 064421 (2014).
- [55] Y. Onose, T. Ideue, H. Katsura, Y. Shiomi, N. Nagaosa, and Y. Tokura, Observation of the magnon Hall effect, *Science* **329**, 297 (2010).
- [56] M. C. Hickey and J. S. Moodera, Origin of Intrinsic Gilbert Damping, *Phys. Rev. Lett.* **102**, 137601 (2009).
- [57] A. Brataas, Y. Tserkovnyak, and G. E. W. Bauer, Scattering Theory of Gilbert Damping, *Phys. Rev. Lett.* **101**, 037207 (2008).
- [58] E. Barati, M. Cinal, D. M. Edwards, and A. Umerski, Gilbert damping in magnetic layered systems, *Phys. Rev. B* **90**, 014420 (2014).
- [59] A. Kamra, R. E. Troncoso, W. Belzig, and A. Brataas, Gilbert damping phenomenology for two-sublattice magnets, *Phys. Rev. B* **98**, 184402 (2018).
- [60] T. Flöss, Quantum fluctuations and magnon-magnon interactions in antiferromagnets, B.S. thesis, Universiteit Utrecht, 2016.
- [61] A. B. Harris, D. Kumar, B. I. Halperin, and P. C. Hohenberg, Dynamics of an antiferromagnet at low temperatures: Spin-wave damping and hydrodynamics, *Phys. Rev. B* **3**, 961 (1971).
- [62] K. P. Sinha and N. Kumar, *Interactions in Magnetically Ordered Solids* (Oxford University Press, New York, 1980).
- [63] P. Wang, L. Lu, and K. Bertoldi, Topological Phononic Crystals with One-Way Elastic Edge Waves, *Phys. Rev. Lett.* **115**, 104302 (2015).
- [64] T. Fukui, Y. Hatsugai, and H. Suzuki, Chern numbers in discretized Brillouin zone: Efficient method of computing (spin) Hall conductances, *J. Phys. Soc. Jpn.* **74**, 1674 (2005).